Supplementary Information for

Improvement of Sensing and Trapping Efficiency of Double Nanohole Apertures via Enhancing the Wedge Plasmon Polariton Modes with Tapered Cusps

Mostafa Ghorbanzadeh[1,2*], *Steven Jones*[2],
Mohammad Kazem Moravvej-Farshi[1], *and Reuven Gordon*[2]

[1]Faculty of Electrical and Computer Engineering, Tarbiat Modares University, P. O. Box 14115-194, Tehran 1411713116, Iran
[2]Department of Electrical and Computer Engineering, University of Victoria, Victoria, BC, Canada, V8P5C2
[*]Email: mghz@uvic.ca; m.ghorbanzadeh@modares.ac.ir

Optical force calculation by FDTD method:

Using the Maxwell's equations and conservation of the linear momentum, we have calculated the applied force on PS nanoparticles. The average of the optical force exerted on a particle is defined as,

$$\overline{\mathbf{F}} = \frac{1}{2}\mathrm{Re}\left[\oint_{\Omega} T(\mathbf{r})\cdot\hat{\mathbf{n}}\, dS\right] \tag{S1}$$

where

$$\mathbf{T}(\mathbf{r}) = \varepsilon\mathbf{E}(\mathbf{r})\otimes\mathbf{E}^{*}(\mathbf{r}) + \mu\mathbf{H}(\mathbf{r})\otimes\mathbf{H}^{*}(\mathbf{r}) - \frac{1}{2}\left(\varepsilon\left|\mathbf{E}(\mathbf{r})\right|^{2} + \mu\left|\mathbf{H}(\mathbf{r})\right|^{2}\right) \tag{S2}$$

is the Maxwell's stress tensor (MST)[1], **r**, and **n** are the position vector, and the unit vector normal to the surface *S*, enclosing the particle volume **Ω,** ε and μ are the medium permittivity and permeability, and **E**, and **H,** are the electric and magnetic field intensity vectors.

Applying a p-polarized plane-wave as the incident optical beam, illuminating the top surface of the DNH, we have used the three dimensional finite difference time domain (3D-FDTD) method to solve the Maxwell's equations for **E** and **H** numerically. The simulation convergence is tested by reducing the mesh-size and extending the simulation region. The boundary conditions, in these calculations, are considered to be perfectly matched layers (PMLs) in all directions. To eliminate the edge effects at the boundaries the total field / scattered field technique has been employed. Next, Eqs. (1) and (2) have been solved, numerically, to obtain the averaged scattering and gradient force components.

Effect of the particles positions on the Optical force components in DNHs with different conical and cylindrical geometries:

Figure S1 shows the wavelength dependencies of the normalized optical forces exerted on a 10nm PS particle positioned at z=−5, 0, 5, 10, 15nm when (i) R_t=70nm, R_b=56nm (i.e., conical DNH: Figure S1a and d, (ii) R_t=R_b=70nm (cylindrical: Figure S1b and e), and (iii) R_t=R_b=56nm (cylindrical: Figure S1c and f). Figures S1a-c and Figures S1d-f show the optical force component, F_x and F_z, leading the particle toward the hot spots. In order to make the comparison logical, the x and y coordinates at which the force components, at any given z are calculated are the same (i.e., y=0 and 20 nm away from the corresponding cusps bottom edge in each DNH).

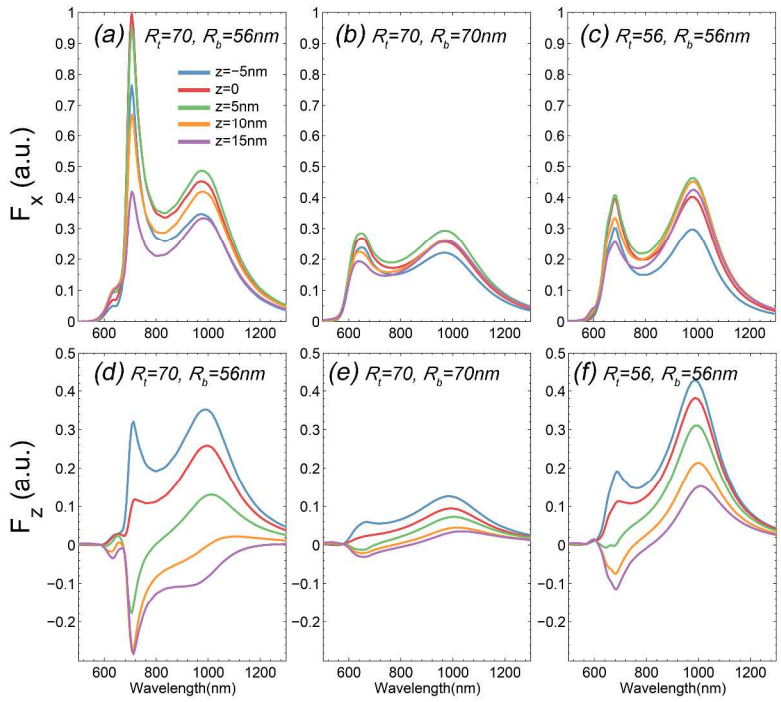

Figure S1. Normalized optical forces components felt by a 10nm PS particle at different z positions within DNH, as functions of the incident wavelengths. The x and y coordinates at which the force components, at any given z are calculated are the same (i.e., y=0 and 20 nm away from the corresponding cusps bottom edge in each DNH).

As can be observed from these illustrations, at the resonance wavelengths of the wedge modes (λ_{WPP}), F_x and $|F_z|$ in the conical DNH are both greater than those at the similar wavelength for both cylindrical DNHs. In other words, the comparison shows that the trapping efficiency of the conical DNH is greater than those of cylindrical DNHs, similar to the observation made from the comparison of the mode intensity profiles as illustrated in Figure 3c. The particle is trapped with an incident light whose wavelength is close to that of the wedge mode, at $z=0^+$ where $F_x>0$ and the component F_z changes sign — i.e., just above the interface of the Au/glass at the wedge corner, tangent to the cusp, also shown in Figure 4c. It is worth mentioning that, in calculating MST, the probe tip should always be in the water (away from the surrounding surfaces). Otherwise, due to the interaction of either of these surfaces with the probe the calculated MST become erroneous.

Effect of substrate milling depth

It is worth nothing that to achieve correct numerical results for transmission variation due to the presence of a nanoparticle, a minimum milling depth into the substrate (T_S) is required. Otherwise (i.e. for $T_S=0$), geometry of the substrate prevents the nanoparticles to be trapped near the WPP hot spots at the DNH bottom cusps. In this case, the interaction between WPP mode and the trapped nanoparticle decreases, which leads to a reduction in the sensitivity of the DNH. Although gold is a soft material and the milling rate of it is larger than that of SiO_2[2–4], in this paper we've considered that the glass in the center of the holes can be milled as much as Au. The reason is that because in fabrication the center of the circles in the DNHs had to be over-milled. In fabrication we used a one-pixel wide line to cut the center of the DNH, and used the same number of passes everywhere for simplicity. Hence, the gap region is cut much less than the center of the DNH circles (where the gold is milled through and then the glass is milled for

several passes). When tuning the number of passes, you can see that it is possible to mill two holes that are disconnected, so as the number of passes is increased the glass beneath the circles is continually milled as the "gap" region becomes just cut through. Nonetheless, according to simulations (see Figure S2) variation of the substrate milling depth from 10 to 100 nm has little effect on the transmission spectrum, especially on the WPP mode because this mode is localized near the bottom cusps and does not penetrate into the depth of the substrate.

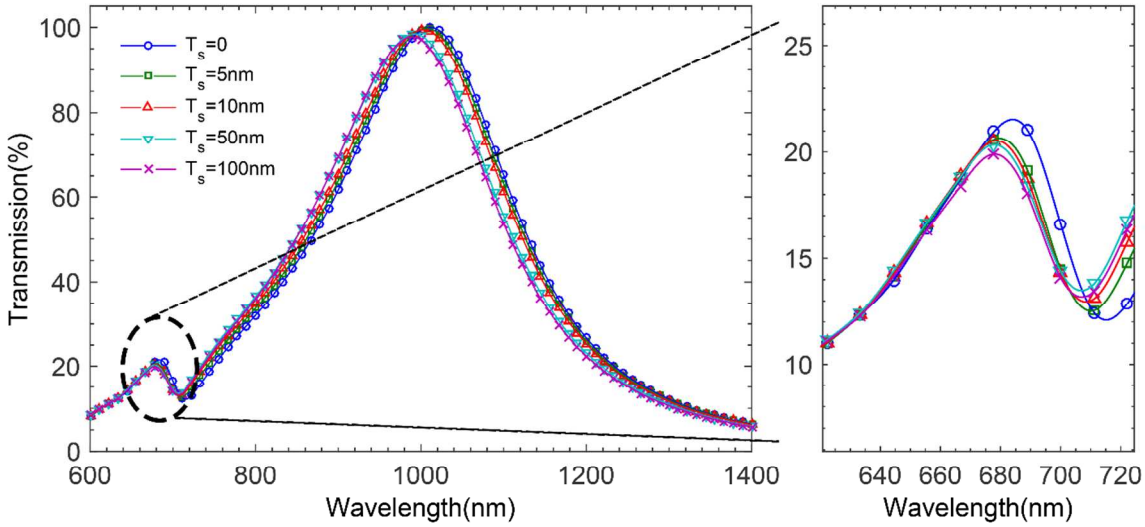

Figure S2. Effect of the substrate milling depth (T_s) on the transmission spectrum when R_t=70nm, R_b=56nm, L=100nm (case(i)).

References

(1) Maier, S. A. *Plasmonics: Fundamentals and Applications*; Springer, 2007.

(2) Bischoff, L.; Teichert, J. Focused Ion Beam Sputtering of Silicon and Related Materials. *Forschungszentrum Rossend.* **1998**.

(3) Jamaludin, F. S.; Mohd Sabri, M. F.; Said, S. M. Controlling Parameters of Focused Ion Beam (FIB) on High Aspect Ratio Micro Holes Milling. *Microsyst. Technol.* **2013**, *19*, 1873–1888.

(4) http://www.specs.de/cms/upload/PDFs/IQE11-35/sputter-Info.pdf.